



University of HUDDERSFIELD

University of Huddersfield Repository

Grossoni, Ilaria, Iwnicki, Simon, Bezin, Yann and Gong, Cencen

Dynamic response of vehicle-track coupling system with an insulated rail joint

Original Citation

Grossoni, Ilaria, Iwnicki, Simon, Bezin, Yann and Gong, Cencen (2013) Dynamic response of vehicle-track coupling system with an insulated rail joint. In: 11th International Conference on Vibration Problems, 9-12 September 2013, Lisbon (Portugal).

This version is available at <http://eprints.hud.ac.uk/id/eprint/23754/>

The University Repository is a digital collection of the research output of the University, available on Open Access. Copyright and Moral Rights for the items on this site are retained by the individual author and/or other copyright owners. Users may access full items free of charge; copies of full text items generally can be reproduced, displayed or performed and given to third parties in any format or medium for personal research or study, educational or not-for-profit purposes without prior permission or charge, provided:

- The authors, title and full bibliographic details is credited in any copy;
- A hyperlink and/or URL is included for the original metadata page; and
- The content is not changed in any way.

For more information, including our policy and submission procedure, please contact the Repository Team at: E.mailbox@hud.ac.uk.

<http://eprints.hud.ac.uk/>

DYNAMIC RESPONSE OF VEHICLE-TRACK COUPLING SYSTEM WITH AN INSULATED RAIL JOINT

Ilaria Grosso¹, Simon Iwnicki¹, Yann Bezin¹, Cencen Gong¹

¹ Institute of Railway Research, University of Huddersfield, Huddersfield, UK

groilla@inwind.it

s.iwnicki@hud.ac.uk

y.bezin@hud.ac.uk

u1273131@hud.ac.uk

Keywords: Rail joints, Impact forces, Dynamic behaviour

Abstract. *The dynamic behavior of vehicle and track systems is studied in the presence of an insulated rail joint through a two-dimensional vehicle-track coupling model. The track system is described as a finite length beam resting on a double layer discrete viscous-elastic foundation. The vehicle is represented through a half car body and a single bogie. These sub-systems are solved independently and coupled together through a Hertzian contact model, where the irregularity caused by the rail joint is modelled as a second order polynomial. A parametric study is carried out in order to understand the influence by the main track and vehicle parameters to the P_1 and P_2 peak forces. Finally, the results in terms of P_2 force from the present model have been compared not only with measured values but also with both other simulated and analytical solutions and an excellent agreement between these values has been found.*

1 INTRODUCTION

There is currently a worldwide trend towards using continuously welded rails for minimizing the wheel-rail impact forces. Nevertheless, rail joints are still used in some areas. In particular, insulated rail joints are required for track electrical insulation to detect the train location and to isolate sections such as those near road crossings.

When a train runs over a joint, large dynamic impact forces are developed which lead to vibrations in the structures and a higher probability of component fatigue and damage. Thus, it is clear that rail joints can affect the maintenance costs, ride comfort and running security on a modern railway.

Many studies have focused on the dynamic response of the railway track under moving vehicles. Some of these [1-4] only consider the track system as a beam on an elastic foundation subjected to moving point loads. Although this approach is simple to implement, it is insufficient to fully model the dynamic behavior of the track and vehicle systems as it neglects the wheel-rail contact aspects. Some other studies [5-8] take the coupling aspects into account, but few [9-10] apply these aspects to model the dynamic behavior in presence of a rail joint.

In this paper, a two-dimensional vehicle-track coupling model is developed. The track system is described as a finite length beam supported on a two-layer discrete elastic foundation. The vehicle is represented using a half car body. These sub-systems are solved independently and coupled together through the Hertzian wheel-rail contact model [5], where the irregularity due to the rail joint is modelled as a second order polynomial. The main results from the parametric study have shown that the first impact force P_1 is greatly influenced by the wheelset mass, the rail mass and the joint angle, whereas the second peak force P_2 is largely affected by the wheelset mass, the rail-pad stiffness, the support stiffness and the joint angle. Finally, the results in terms of the P_2 force from this model have been compared not only with measured data [9] but also with both other simulated [9] and analytical [11-12] solutions. An excellent agreement has been found in all the comparisons.

2 MODELLING THE VEHICLE-TRACK COUPLING SYSTEM

The vehicle-track coupling model with an insulated rail joint is shown in Figure 1.

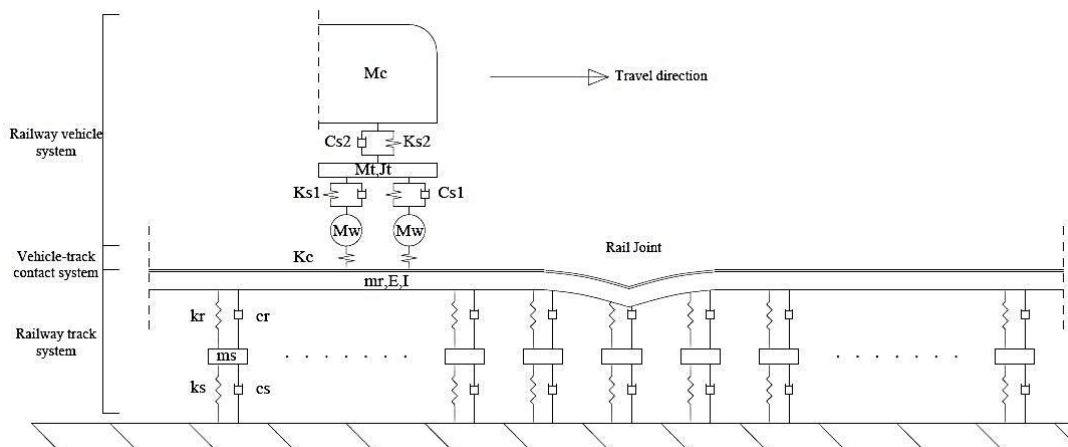


Figure 1: Vehicle-track coupling model with an insulated rail joint.

2.1 Fundamental assumptions

The main assumptions are listed as follows:

- 1) Only vertical dynamic forces are considered in the model. Due to the track symmetry, it is possible to use a single rail in the calculation.
- 2) The track system is modelled through a two-layer discretely supported ballast track model. A finite straight track without imperfections is considered. The number of beam elements considered is 40, because in this way it is possible to avoid the overlapping between the increasing static load during the transient time and the dynamic forces due to the rail joint.
- 3) A half car body is considered in the vehicle model. All the masses are assumed to be concentrated in the centre of gravity of the corresponding element. The two wheelsets masses and profiles are assumed to be the same.
- 4) The classical Hertzian contact model is used to couple the vehicle and track models.
- 5) The rail joint is modelled through a second order polynomial as established by a comparison between a quadratic fit function and the experimental measurements [13].
- 6) The joint fishplates contribution to the local stiffness is neglected.
- 7) It is assumed that there is one contact point at each wheel.

2.2 Modelling the track system

The moving force is characterized by a constant value of speed S , thus the simple formula for the uniform linear motion has been used. A finite element (FE) analysis is developed approximating the deformation within an element through using nodal values of displacement and rotation.

The beam has uniform flexural rigidity EI and mass per unit length \bar{m}_r . The sleepers are represented by their effective mass m_s , and assumed to be concentrated in the centre of gravity. The support is represented by rail-pad and ballast. The rail-pad is characterized by a spring of stiffness k_r in parallel with a damper having viscous damping coefficient c_r , while the ballast layer is similarly represented by a spring of stiffness k_s and a damper in parallel with constant c_s .

2.3 Modelling the vehicle system

The model used here consists of a quarter car supported by a bogie through the secondary suspension and a bogie supported by two half wheelsets through the primary suspension. All the bodies are assumed to be rigid. The car body is represented by its mass M_c , the bogie by its mass M_t and its pitch moment of inertia J_t and the wheelset by its mass M_w . Each primary suspension is modelled as a spring of stiffness K_{s1} in parallel with a damper with viscous constant C_{s1} . Similarly, the secondary suspension is characterized by a spring of stiffness K_{s2} in parallel with a dashpot having viscous constant C_{s2} .

3 RESULTS

In order to solve the coupling system, the track parameters used are reported in Table 1.

| Variable | Value | Variable | Value |
|--|--|-------------------------------------|---------------------------|
| Mass per length unit (UIC60) \bar{m}_r | 60.21 [kg/m] | Car body mass M_c | 13000 [kg] |
| Moment of inertia (UIC60) I_{yy} | $3.04 \cdot 10^{-5}$ [m ⁴] | Bogie mass M_t | 1600 [kg] |
| Young's modulus of rail E | $2.11 \cdot 10^{11}$ [N/m] | Bogie pitch moment of inertia J_t | 1560 [kg·m ²] |
| G44 concrete sleeper | 308 [kg] | Wheelset mass M_w | 700 [kg] |

| Variable | Value | Variable | Value |
|------------------------------------|-------------------------|---|--|
| mass m_s | | Primary suspension stiffness K_{s1} | $1.87 \cdot 10^6$ [N/m] |
| Pandrol rail-pad stiffness k_r | $2.70 \cdot 10^8$ [N/m] | Primary suspension damping C_{s1} | $5 \cdot 10^5$ [N·s/m] |
| Pandrol rail-pad damping c_r | $2 \cdot 10^5$ [N·s/m] | Secondary suspension stiffness K_{s2} | $1.72 \cdot 10^6$ [N/m] |
| Typical support stiffness k_s | $8 \cdot 10^7$ [N/m] | Secondary suspension damping C_{s2} | $1.96 \cdot 10^5$ [N·s/m] |
| Typical support damping c_s | $1 \cdot 10^5$ [N·s/m] | Distance between the centre of pivot and the centre of wheelset l_t | 1.25 [m] |
| Sleeper spacing l | 0.65 [m] | Wheel rolling radius r_0 | 0.46 [m] |
| Number of beam elements n | 40 | Hertzian contact constant for worn wheels G | $4.22 \cdot 10^{-8}$ [m/N ^{2/3}] |
| Maximum joint depth D | 0.01 [m] | Newmark Beta parameter α | 0.25 |
| Affecting length of rail joint L | 3.65 [m] | Newmark Beta parameter β | 0.50 |
| Travelling speed S | 160 [km/h] | Wilson Theta parameter θ | 1.40 |
| Time step Δt | $5 \cdot 10^{-4}$ [s] | | |

Table 1: Track parameters [14], vehicle parameters [15], wheel-rail contact parameters [15], rail joint parameters [10] and integration parameters.

The response in term of wheel-rail contact force versus time is shown in Figure 2. It can be deduced that the results from the Wilson Theta integration method are higher than those from the Newmark Beta integration method. The peak difference is about 15%.

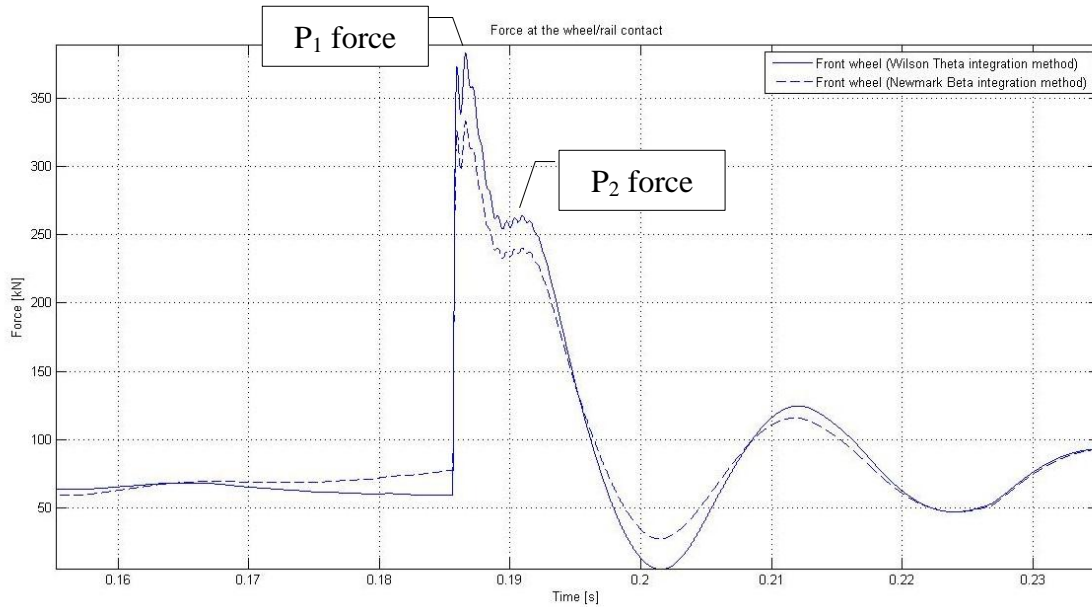


Figure 2: Wheel-rail contact force versus time.

It is also possible to recognize two impact forces (P_1 and P_2 forces).

The P_1 force is a high frequency force (approximately 500 Hz) and it is characterized by high magnitude, which is found approximately 5 times bigger than the unsprung static load. It is associated mainly to the battering of the unsprung mass on the rail-end and is absorbed mainly by the rail and sleeper inertias. In the example shown in Figure 2, the force peak occurs 0.3 ms after crossing the joint, which is within the typical range between 0.25 ms and 0.5 m [11].

The P_2 force, which occurs several milliseconds after the impact, is a medium frequency force (approximately 30-40 Hz) and its peak is lower than the P_1 , around 3-3.5 times bigger than the static force. Contrary to the P_1 force, the P_2 force depends on the rail bending resilience and it is transmitted to the ballast, producing an acceleration of deterioration of the whole track system. This is the reason why the vehicle designers should reduce the unsprung masses as much as possible.

The P_1 and P_2 forces can be determined in the first approximation as in Eqs. (1-2) [11]:

$$P_1 = P_0 + 2\alpha V \sqrt{\frac{K'_H m_e}{1 + \frac{m_e}{m_u}}} \quad (1)$$

$$P_2 = P_0 + 2\alpha V \cdot \left(1 - \frac{c_t \pi}{4k_t(m_t + m_u)}\right) \cdot \sqrt{\frac{1}{1 + \frac{m_t}{m_u}} \cdot k_t m_u} \quad (2)$$

Where P_0 is the static wheel load, 2α the total joint angle, V the travelling speed, K'_H the linearized Hertzian contact stiffness, P the generic load value, G the Hertzian contact constant, m_u the unsprung mass, m_e the effective track mass and m_t , k_t and c_t the equivalent track system parameters defined in [11].

The UK standard GM/TT0088 states that “vehicles shall be able to run over the normal range of vertical track irregularities at normal operating speeds without generating excessive vertical loads and stresses in the rails and track” [12]. There is a limit only for the P_2 force, which cannot exceed a total value of 322 kN per wheel at the maximum operative speed. This limit is made because this force is directly transmitted to the ballast, as said previously. In particular, an analytic formula has been proposed as in Eq. (3) [12]:

$$P_2 = Q + A_z \cdot V_m \cdot M \cdot C \cdot K \quad (3)$$

Where Q is the maximum static wheel load, V_m the maximum normal operating speed, M_v the effective vertical unsprung mass per wheel, M , C and K parameters reported in [12].

3.1 Parametric study

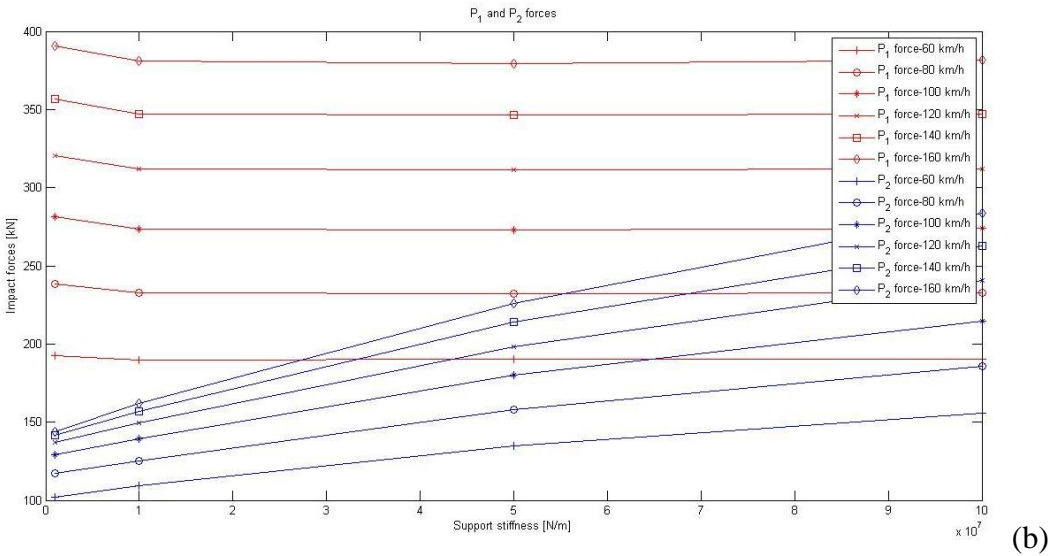
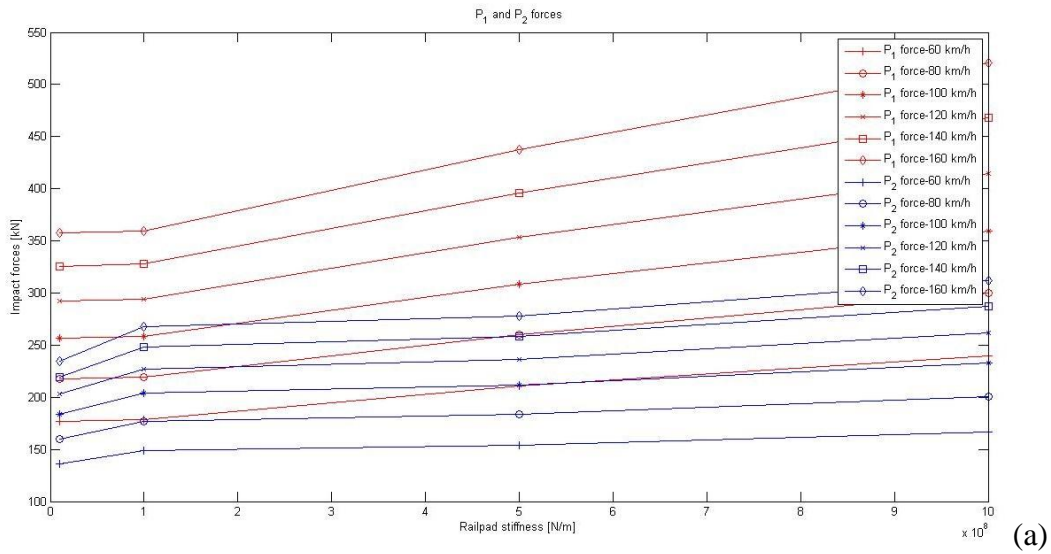
Numerical examples are shown and the effects of some parameters are investigated. The parameters of track, vehicle and joint models which have been used in the simulation are reported in Table 2.

| | Track model | Vehicle model | Joint model |
|------------|---------------------------------------|-----------------------------|-----------------------------|
| Parameters | Travelling speed S | Travelling speed S | Travelling speed S |
| | Rail mass per unit length \bar{m}_r | Wheelset mass M_w | Affected length L |
| | Rail-pad stiffness k_r | Bogie mass M_t | Total joint angle 2α |
| | Support stiffness k_s | Car body mass M_c | |
| | Total joint angle 2α | Total joint angle 2α | |

Table 2: Parameters of simulations.

The integration method used is the Wilson Theta method because it gives higher values compared to the Newmark Beta method, as shown in Figure 2.

In the following, only the most relevant graphs are reported.



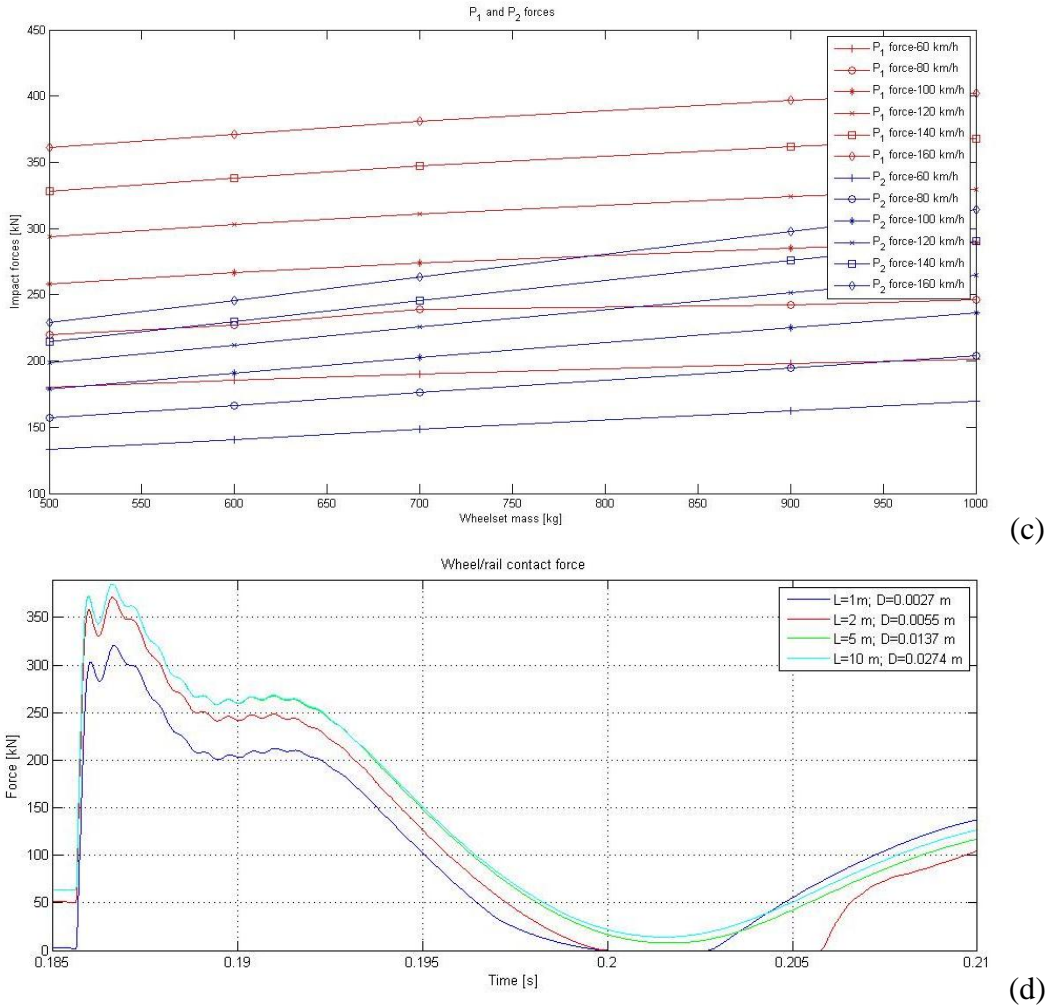


Figure 3: The variation of P₁ (red lines) and P₂ (blue lines) forces with (a) rail-pad stiffness; (b) support stiffness; (c) wheelset mass; (d) joint shape fixing the total joint angle.

From Figure 3-a, it is found that the trends of P₁ and P₂ forces with the rail-pad stiffness are different. In the case of P₁ force, there is a first constant trend for low stiffness values (10^7 - 10^8 N/m) and then a linearly increasing trend for higher stiffness ($5 \cdot 10^8$ - 10^9 N/m). The slope increases with increasing speed, from about 25% in the case of 60 km/h to about 32% in the case of 160 km/h. In case of P₂ force, instead, there is a relatively rapid increasing trend for low stiffness values (10^7 - 10^8 N/m) and then a relatively slower increasing trend for higher stiffness ($5 \cdot 10^8$ - 10^9 N/m) with a slope significantly lower than the first part.

Regarding the support stiffness (Figure 3-b), it can be found that the P₁ trend is relatively constant while the P₂ grows linearly. The average slope increases with increasing travelling speed, from about 35% at 60 km/h to about 50% at 160 km/h. This means that decreasing the ballast stiffness has little effect on the P₁ force, whereas it can reduce the P₂ force.

As shown in Figure 3-c, the impact of the wheelset mass is very large in both cases. In particular, the P₁ force trend is asymptotic, that is the change of wheelset mass plays a limited role in that impact force for values greater than 600-800 kg. The P₂ force increases proportionally with the wheelset mass, with the average slope increasing with increasing travelling speed.

Finally, from Figure 3-d it can be deduced that both the impact forces are different in case of different affected length L. Thus, the dynamic response in terms of wheel-rail contact

forces is closely related to the actual shape of the rail joint. This conclusion is against the formulae proposed by the UK researchers in Eqs. (1-2), according to which the forces are constant for constant value of total dip angle. Therefore, those formulae can give only a rough estimation of the forces.

3.2 Comparison

The main characteristics of two different Chinese freight vehicles, C62A and C75, are reported in Table 3.

| Variable | C62A | C75 |
|---|------------------------------------|------------------------------------|
| Car body mass M_c | 19250 [kg] | 22950 [kg] |
| Bogie mass M_t | 565 [kg] | 755 [kg] |
| Bogie pitch moment of inertia J_t | 380 [$\text{kg}\cdot\text{m}^2$] | 780 [$\text{kg}\cdot\text{m}^2$] |
| Wheelset mass M_w | 600 [kg] | 647.5 [kg] |
| Primary suspension stiffness K_{s1} | - | - |
| Primary suspension damping C_{s1} | - | - |
| Secondary suspension stiffness K_{s2} | $1.06\cdot 10^7$ [N/m] | $1\cdot 10^7$ [N/m] |
| Secondary suspension damping C_{s2} | $1.40\cdot 10^5$ [Ns/m] | $1\cdot 10^5$ [Ns/m] |
| Distance between the centre of pivot and the centre of wheelset l_t | 0.87 [m] | 0.87 [m] |
| Wheel rolling radius r_0 | 0.42 [m] | 0.42 [m] |

Table 3: Main characteristics of C62A and C75 freight vehicles [9].

In Figure 4 the comparison between the results in terms of P_2 force in case of C62A and C75 freight vehicles with increasing travelling speed is shown. In particular, for each travelling speed and each vehicle type five different values of the peak force are considered: measured data [9], simulated value [9], two different analytic solutions [11-12] and the present model.

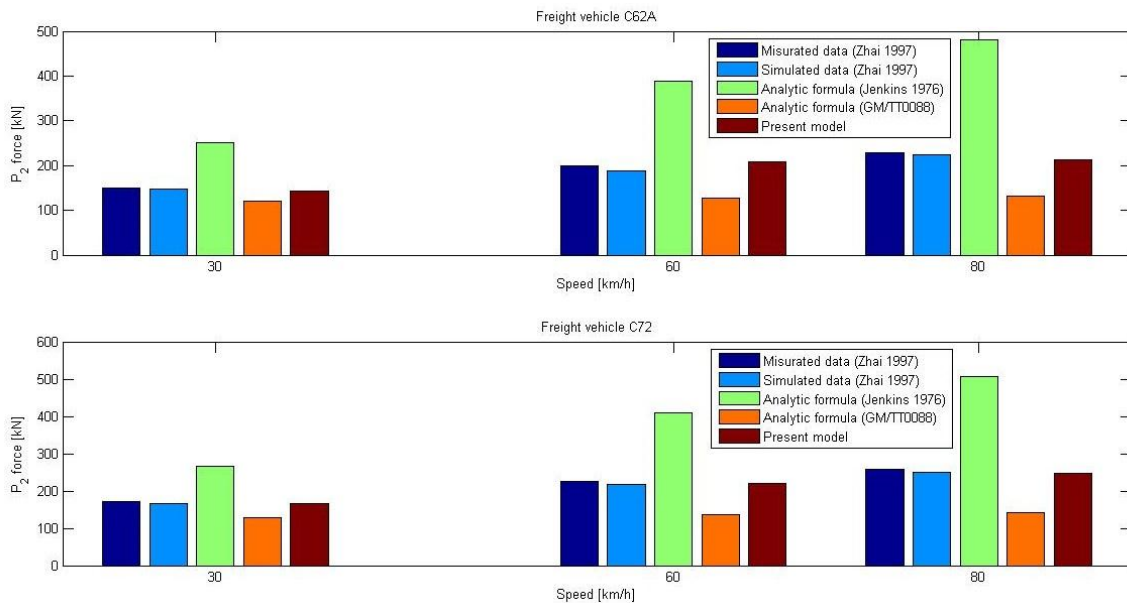


Figure 4: Comparison between the results in terms of P_2 force in case of C62A and C75 freight vehicles.

It is noticeable that the results are close to each other, particularly the measured data, simulated values and the present model. The percentage differences between the present model and measured data or simulated values are reported in Table 4.

| Travelling speed [km/h] | C62A | | C75 | |
|-------------------------|-------------------|----------------------|-------------------|----------------------|
| | Measured data [%] | Simulated values [%] | Measured data [%] | Simulated values [%] |
| 30 | 4.5 | 3.2 | 3.2 | 0.8 |
| 60 | 3.7 | 10.9 | 2.2 | 1.6 |
| 80 | 6.5 | 4.4 | 3.7 | 0.6 |

Table 4: Percentage differences between the present model, the measured data and the simulated values.

4 CONCLUSIONS

The primary objective of this paper is to investigate the characteristics of vertical dynamic response due to insulated rail joint (IRJ) through developing a comprehensive finite element (FE) model of vehicle-track coupling system. The two dimensional model employed has been established by merging three elementary models, which are the track model, the vehicle model and the contact model. This strategy was proven efficient to obtain an efficient solution. Two explicit numerical integration methods have been employed in the dynamic analysis. In order to achieve a reasonable model size which is compatible to the available computing facility, several assumptions have been made in the rail joint model, track model and boundary conditions.

The wheel-rail impact mechanism can be explained through the stiffness discontinuity of the IRJ structure. The joint causes a geometric discontinuity in the running surface during the wheel passage, which therefore produces the impact in the vicinity of the gap. At impact, two peak contact forces develop. The main characteristics, such as the frequency and the magnitude, are quite different. It has been demonstrated that the lower magnitude force is the force that actually causes the track degradation because its characteristic frequencies match with the track frequencies.

Through a series of sensitivity studies of several parameters, it was shown that the dynamic response can be largely improved by optimised design parameters. The parametric simulations have shown that the first impact force P_1 is greatly influenced by the wheelset mass, the rail mass and the joint angle, whereas the second peak force P_2 is affected by the wheelset mass, the rail-pad stiffness, the support stiffness and the joint angle. The model has outlined that the impact forces depends on the actual shape of the rail joint. Therefore, great reductions of peak forces values can be obtained through an appropriate joint design.

Finally, the results in terms of P_2 force from the present model have been compared not only with measured values but also with both simulated and analytical solutions. An excellent agreement between values has been found, with a maximum percentage difference of 10%.

REFERENCES

- [1] P. Lou, Q. Zeng, Finite element analysis of infinitely long beam resting on continuous viscoelastic foundation subjected to moving loads. *Journal of Traffic and Transportation Engineering*, **3**(2), 1-6, 2003.
- [2] D. Thambiratnam and Y. Zhuge, Dynamic analysis of beams on an elastic foundation subjected to moving loads. *Journal of Sound and Vibration*, **198**, 149-169, 1996.

- [3] Y. Wang, et al., Transient responses of beam with elastic foundation supports under moving wave load excitation. *International Journal of Engineering Science and Technology*, **1**, 137-143, 2011.
- [4] S.L. Grassie, et al., The dynamic response of railway track to high frequency vertical excitation. *Journal of Mechanical Engineering Science*, **24**, 77-90, 1982.
- [5] X. Lei, and N.A. Noda, Analyses of dynamic response of vehicle and track coupling system with random irregularity of track vertical profile. *Journal of Sound and Vibration*, **258**, 147-165, 2002.
- [6] W. Zhai, et al., Fundamentals of vehicle-track coupled dynamics. *Vehicle System Dynamics*, **47**, 1349-1376, 2009.
- [7] F. Lu, et al., Symplectic analysis of vertical random vibration for coupled vehicle-track systems. *Journal of Sound and Vibration*, **317**, 236-249, 2008.
- [8] G. Diana, et al., Modelli matematici per lo studio dell'interazione veicolo-struttura-armamento. *Ingegneria Ferroviaria*, **12**, 1066-1080, 1995.
- [9] W. Zhai, and Z. Cai, Dynamic interaction between a lumped mass vehicle and a discretely supported continuous rail track. *Computers and Structures*, **63**, 987-997, 1997.
- [10] R.V. Dukkipati, and R. Dong, The dynamic effects of conventional freight car running over a dipped-joint. *Vehicle System Dynamics*, **31**(2), 95-111, 1999.
- [11] H.H. Jenkins, et al., The effect of track and vehicle parameters on wheel-rail vertical dynamic forces. *Railway Engineering Journal*, **1**, 2-22, 1974.
- [12] British Railways Board, *Permissible track forces for railway vehicles*, Group Standards Railway Technical Centre (Derby), 1993.
- [13] T.X. Wu and D.J. Thompson, On the impact noise generation due to a wheel passing over rail joints. *Journal of Sound and Vibration*, **267**, 485-496, 2003.
- [14] Y. Bezin, *An integrated flexible track system model for railway vehicle dynamics*. PhD thesis, Manchester Metropolitan University, Manchester, 2008.
- [15] W.M. Zhai, *Vehicle-track coupling dynamics*. Science Press, Beijing, 2007.